Article

Edge Epitaxy of Two-dimensional MoSe2 and MoS2 Nanosheets on One-dimensional Nanowires

Junze Chen, Xue-Jun Wu, Yue Gong, Yihan Zhu, Zhenzhong Yang, Bing Li, Qipeng Lu, Yifu Yu, Shikui Han, Zhicheng Zhang, Yun Zong, Yu Han, Lin Gu, and Hua Zhang

J. Am. Chem. Soc., **Just Accepted Manuscript** • Publication Date (Web): 05 Jun 2017

Edge Epitaxy of Two-dimensional $MoSe_2$ and MoS_2 Nanosheets on One-dimensional Nanowires

Junze Chen,[†,‡] Xue-Jun Wu,[†,‡] Yue Gong,[Δ,‡] Yihan Zhu,[§,‡] Zhenzhong Yang,[Δ] Bing Li,[⊥] Qipeng Lu,[†] Yifu Yu,[†] Shikui Han,[†] Zhicheng Zhang,[†] Yun Zong,[⊥] Yu Han,*[,§] Lin Gu,*[,Δ,¤,□] and Hua Zhang*[,†]

[†]Center for Programmable Materials, School of Materials Science and Engineering, Nanyang Technological University, 50 Nanyang Avenue, Singapore 639798, Singapore.

[Δ]Beijing National Laboratory for Condensed Matter Physics, Institute of Physics, Chinese Academy of Sciences, Beijing 100190, China.

[§]Advanced Membranes and Porous Materials Center, Physical Sciences and Engineering Division, King Abdullah University of Science and Technology, Thuwal 23955-6900, Kingdom of Saudi Arabia.

[⊥]Institute of Materials Research and Engineering (IMRE), A*STAR (Agency for Science, Technology and Research), 2 Fusionopolis Way, Innovis #08-03, Singapore 138634, Singapore.

[¤]Collaborative Innovation Center of Quantum Matter, Beijing 100190, China.

[□]School of Physical Sciences, University of Chinese Academy of Sciences, Beijing 100190, China.

ABSTRACT

Rational design and synthesis of heterostructures based on transition metal dichalcogenides (TMDs) have attracted increasing interests because of their promising applications in electronics, catalysis, etc. However, the construction of epitaxial heterostructures with interface at the edges of TMD nanosheets (NSs) still remains great challenge. Here, we report a strategy for controlled synthesis of a new type of heterostructures in which TMD NSs, including MoS_2 and $MoSe_2$, vertically grow along the longitudinal direction of one-dimensional (1D) $Cu_{2-x}S$ nanowires (NWs) in an epitaxial manner. The obtained $Cu_{2-x}S$-TMD heterostructures with tunable loading amount and lateral size of TMD NSs are achieved by the consecutive growth of TMD NSs on $Cu_{2-x}S$ NWs through the gradually injection of chalcogen precursors. After cation exchange of Cu in $Cu_{2-x}S$-TMD heterostructures with Cd, the obtained CdS-MoS_2 heterostructures remained their original architectures. Compared to the pure CdS NWs, the CdS-MoS_2 heterostructures with 7.7 wt% loading of MoS_2 NSs exhibit the best performance in the photocatalytic hydrogen evolution reaction with the H_2 production rate up to 4,647 $\mu mol \cdot h^{-1} \cdot g^{-1}$, about 58 times that catalyzed with pure CdS NWs. Our synthetic strategy opens up a new way for the controlled synthesis of TMD-based heterostructures which could have various promising applications.

KEYWORDS: Epitaxial growth, MoS_2, $MoSe_2$, Heterostructure, Hydrogen evolution, Photocatalysis

1. INTRODUCTION

Heterostructures, integrating distinct components with different functionalities in one system, have attracted tremendous attention due to their fascinating properties and various potential applications.[1-5] Among the methods for preparation of heterostructures, epitaxial growth[6] is an effective strategy for construction of novel heterostructures with promising applications in electronics,[7-9] optoelectronics,[10-12] thermoelectronics,[13,14] and catalysis.[15,16] For example, recently two-dimensional (2D) transition metal dichalcogenide (TMD) nanosheets (NSs) have been used as a platform for construction of heterostructures through the vertically or laterally epitaxial growth of other nanomaterials.[17-20] However, the epitaxial growth of lateral heterostructures at the edges of TMD NSs still remains a great challenge, since there are limited materials with lattice parameters matching the edges of TMDs. Until now, only a few lateral heterostructures have been reported, including MoS_2–$MoSe_2$,[21] MoS_2–WS_2,[22,23] $MoSe_2$-WS_2,[24] $MoSe_2$–WSe_2[25] and WS_2–WSe_2.[21] However, both components in the aforementioned lateral heterostructures are limited to TMD NSs. The aforementioned lateral heterostructures with unique optical and electrical properties are key components for construction of *p*-*n* rectifying diodes, light-emitting diodes, photovoltaic devices and transistors.[21-25] To the best of our knowledge, there is no report on the preparation of epitaxial heterostructures with interface at the edges of TMD NSs and other non-layered nanomaterials.

Here, we report a wet chemical method for the controlled synthesis of a new type of heterostructures, in which 2D TMD NSs, i.e. MoS_2 and $MoSe_2$, are vertically grown along the longitudinal direction of one-dimensional (1D) $Cu_{2-x}S$ nanowires (NWs) in an epitaxial manner. The lateral size of synthesized TMD NSs can be well tuned from less than 2 nm to ~10 nm by changing the amount of injected chalcogen precursors. After the cation exchange of Cu in the

synthesized $Cu_{2-x}S$-MoS_2 heterostructures with Cd, the architectures of obtained CdS-MoS_2 heterostructures are well maintained. As a proof-of-concept application, the CdS-MoS_2 heterostructures with different loading amount of MoS_2 are used for the photocatalytic hydrogen evolution reaction (HER) under the visible light irradiation (>420 nm). It is found that the rate of H_2 evolution catalyzed with CdS-MoS_2 heterostructures with 7.7 wt% loading of MoS_2 is up to 4,647 $\mu mol \cdot h^{-1} \cdot g^{-1}$, which is about 58 times that catalyzed with pure CdS NWs.

2. EXPERIMENTAL SECTION

Chemicals and Materials. Cadmium acetate dihydrate [$Cd(Ac)_2 \cdot 2H_2O$, 98%, Alfa Aesar], copper(II) chloride dihydrate ($CuCl_2 \cdot 2H_2O$, ACS reagent, >99.0%, Sigma-Aldrich), diphenyl diselenide (PDSe, 98%, Sigma-Aldrich), bis(acetylacetonato)dioxomolybdenum(VI) [$MoO_2(acac)_2$, Sigma-Aldrich], sulfur powder (−100 mesh, refined, Sigma-Aldrich), tert-Dodecylmercaptan (t-DDT, 98%, Sigma-Aldrich), ethylenediamine (absolute, >99.5%, Sigma-Aldrich), oleic acid (OA, 90%, Sigma-Aldrich), oleylamine (OM, technical grade, 70%, Sigma-Aldrich), 1-octadecene (ODE, technical grade, 90%, Sigma-Aldrich), trioctylphosphine (TOP, 97%, Sigma-Aldrich), triethanolamine (TEA, 98%, Sigma-Aldrich), ammonium sulfide solution [$(NH_4)_2S$, 20% in water, Sigma-Aldrich], toluene (99.8%, Sigma-Aldrich), acetone (technical grade), and methanol (AR) were used as received without further purification. The Milli-Q water (Milli-Q System, Millipore, Billerica, MA) was used in the photocatalytic hydrogen evolution experiment.

Synthesis of CdS nanowires (NWs). The CdS NW was synthesized according to a reported solvethermal method with slight modification.[26] Briefly, 0.3 mmol of $Cd(Ac)_2 \cdot 2H_2O$ and 1.0 mmol of sulfur powder were added into 9 mL ethylenediamine and then stirred for 20 min to

form a yellow dispersion. The dispersion was transferred into an autoclave (volume 23 mL) and kept in the oven at 200 ºC for 3 h. After being cooled down to room temperature, the product was collected by centrifugation at 6,000 r.p.m for 3 min, washed with ethanol for 3 times, and finally dispersed in 6 mL OM.

Synthesis of $Cu_{2-x}S$ NWs through the cation exchange of CdS NW. 1.0 mmol of $CuCl_2 \cdot 2H_2O$ was added into 10 mL OM in a 100 mL three-neck flask. The slurry was degassed upon heating at 120 ºC under vacuum with vigorous magnetic stirring for 30 min. The mixture was purged with nitrogen and heated to 150 ºC to produce a clear yellow solution. 0.1 mmol of CdS NW dispersion in 2 mL OM was quickly injected into the aforementioned solution. The temperature suddenly dropped to 140 ºC, and it was heated back to 150 ºC. After 10 min, the mixture was cooled down to room temperature. The obtained $Cu_{2-x}S$ NWs were collected by centrifugation at 6,000 r.p.m for 3 min, and then washed with toluene for three times.

Synthesis of $Cu_{2-x}S$-$MoSe_2$ heterostructure. 0.1 mmol of $Cu_{2-x}S$ NW and 0.1 mmol of $MoO_2(acac)_2$ were added into 15 mL OM in a 100 mL three-neck flask. The slurry was degassed upon heating at 120 ºC under vacuum with vigorous magnetic stirring for 30 min. After the mixture was purged with nitrogen for another 30 min, it was heated to 200 ºC, referred to as Solution 1. In a 20 mL vial, 0.5 mmol of PDSe were added into 10 mL OM with magnetic stirring to get a clear yellow solution. The solution was purged with nitrogen for 30 min and then sealed it, which was defined as PDSe/OM (0.05 M) stock solution. 1.75 mL of PDSe/OM (0.05 M) stock solution were added into the aforementioned Solution 1 by using a syringe pump at a speed of 0.5 mL/h. After desired volume of the stock solution was introduced, the mixture was cooled down to room temperature to get $Cu_{2-x}S$-$MoSe_2$ heterostructures with different loading

amount of $MoSe_2$. The product was collected by centrifugation at 6,000 r.p.m for 3 min, and then washed with toluene for three times. The obtained product can be well dispersed in toluene.

Synthesis of $Cu_{2-x}S$-MoS_2 heterostructures. The procedures for synthesis of $Cu_{2-x}S$-MoS_2 heterostructures were similar with those for synthesis of $Cu_{2-x}S$-$MoSe_2$ heterostructures. 0.1 mmol of $Cu_{2-x}S$ NW and 0.1 mmol of $MoO_2(acac)_2$ were added to 15 mL OM in a 100 mL three-neck flask at room temperature. The slurry was degassed upon heating at 120 ºC under vacuum with vigorous magnetic stirring for 30 min. After the mixture was purged with nitrogen for another 30 min, it was heated to 200 ºC, referred to as Solution 2. The S precursor, which defines as t-DDT/OM stock solution, was prepared by mixing 235 μL of t-DDT in 2.265 mL OM in a 10 mL vial, which was then purged with nitrogen for 30 min and sealed. 2 mL of t-DDT/OM stock solution were added into the aforementioned Solution 2 by using a syringe pump at a speed of 0.25 mL/h. After desired volume of stock solution was introduced, the mixture was cooled down to room temperature to get $Cu_{2-x}S$-MoS_2 heterostructures with different loading amount of MoS_2. The product was collected by centrifugation at 6,000 r.p.m for 3 min, and then washed by toluene for three times. The obtained product can be well dispersed in toluene.

Synthesis of CdS-MoS_2 heterostructures by the cation exchange of $Cu_{2-x}S$-MoS_2 heterostructures. 1.0 mmol of CdO was added into a mixture of 4 mL OA and 6 mL ODE in a 100 mL three-neck flask. The slurry was degassed upon heating at 120 ºC under vacuum with vigorous magnetic stirring for 30 min. The mixture was then purged with nitrogen and heated to 230 ºC to produce a clear solution. The solution was cooled down to 180 ºC. 0.1 mmol of $Cu_{2-x}S$-MoS_2 dispersed in 3 mL OM was quickly injected to the aforementioned solution, followed by injection of 1 mL TOP. After keeping at 180 ºC for 15 min, the mixture was cooled down to

room temperature. The CdS-MoS_2 heterostructures were collect by centrifugation at 6,000 r.p.m for 3 min, and then washed with toluene for three times.

Characterization. X-ray diffraction (XRD) patterns of the dried products were recorded on Bruker D8 diffractometer with a slit of (1/2)° at a scanning rate of 1° min^{-1}, using Cu Kα radiation (λ = 1.5406 Å). Samples for transmission electron microscopy (TEM) characterizations were prepared by dropping the heterostructures dispersion in toluene on amorphous carbon-coated copper grids. TEM characterization was performed with JEOL 2100F (Japan) operated at 200 kV. High-resolution TEM (HRTEM) images were recorded on a FEI-Titan ST electron microscope operated at 300 kV. Scanning transmission electron microscopy (STEM) and energy-dispersive X-ray spectroscopy (EDS) element mapping images were obtained by a JEOL ARM200F (JEOL,Tokyo, Japan) operated at 200 kV with cold field emission gun and double hexapole Cs correctors (CEOS GmbH, Heidelberg, Germany). Inductively coupled plasma optical emission spectrometry (ICP-OES) was performed on a Dual-view Optima 5300 DV ICP-OES system. X-ray photoelectron spectroscopy (XPS) measurements were carried out on a VG ESCALAB 220I-XL system.

Phase transfer of CdS-MoS_2 heterostructures into water. The as-prepared CdS-MoS_2 heterostructures were transferred into water by using the $(NH_4)_2S$-assisted phase transfer method. After 20 mg of CdS-MoS_2 heterostructures in 5 mL toluene were added into a 10 mL glass vial, 0.5 mL of $(NH_4)_2S$ water solution (10 wt%) together with 0.5 mL of methanol were then added with vigorous stirring. After 5 min, the CdS-MoS_2 heterostructures were transferred into water phase. The water-soluble CdS-MoS_2 heterostructures were collected by centrifugation at 6,000 r.p.m for 3 min and the washed three times with methanol.

Photocatalytic hydrogen Evolution. The photocatalytic activity was evaluated by using water-soluble CdS-MoS_2 heterostructures as photocatalyst. 5 mg of CdS-MoS_2 photocatalyst were suspended in 10 mL aqueous solution containing 10 vol% of TEA used as the sacrificial agent. The suspension was sealed in a quartz vessel and purged with nitrogen for 30 min to remove oxygen. After that, the vessel was exposed under a 300 W Xenon lamp (MAX-302, Asahi Spectra Company, Led.) coupled with a UV cut-off filter (>420 nm) to evaluate the photocatalytic activity under the visible-light irradiation. The H_2 product was analyzed periodically by gas chromatograph (GC, Agilent 7890A) with a thermal conductivity detector (TCD).

3. RESULTS AND DISCUSSION

The $Cu_{2-x}S$-MoX_2 (X=S or Se) heterostructures were synthesized by a seeded-mediated growth method, in which the $Cu_{2-x}S$ NWs, obtained from the transformation of CdS NWs, were used as the seeds (Fig. 1a, see Experimental Section for details). By using the reported solvethermal method with slight modification,[26] CdS NWs with diameter of about 30–50 nm and length of about 1–3 μm were synthesized (Fig. S1). After cation exchange of CdS NWs, the obtained $Cu_{2-x}S$ NWs still kept the 1D morphology and their crystalline structure was confirmed by XRD and TEM (Fig. S2). To fulfill the directional growth of TMD NSs on 1D $Cu_{2-x}S$ NWs, the chalcogen precursor solution was slowly injected with a syringe pump into a mixture, containing 1D $Cu_{2-x}S$ NW seeds, molybdenum precursor and oleylamine, at 200 ºC. Fig. 1b shows a typical high-angle annular dark-field STEM (HAADF-STEM) image of the as-obtained $Cu_{2-x}S$-$MoSe_2$ heterostructure, in which the high-density $MoSe_2$ NSs vertically grow along the longitudinal direction of 1D $Cu_{2-x}S$ NWs (See TEM images and XRD patterns in Fig. S3 and Fig. S4,

respectively). The successful preparation of $Cu_{2-x}S$-$MoSe_2$ heterostructures was further confirmed by XPS (Fig. S5). The HRTEM image (Fig. 1c) clearly shows that the as-prepared $Cu_{2-x}S$-$MoSe_2$ heterostructures are consisted of three components, i.e. (i) djurleite $Cu_{1.94}S$, (ii) high chalcocite Cu_2S, and (iii) $MoSe_2$ NSs, which are well identified from the corresponding fast Fourier transformation (FFT) pattern (the inset of Fig. 1c). The selected area electron diffraction (SAED) pattern indicates that the major component of $Cu_{2-x}S$-$MoSe_2$ heterostructures is the djurleite $Cu_{1.94}S$ (i), consistent with the simulate electron diffraction pattern (Fig. S6). The FFT patterns taken at the circles (i) and (ii), and square (iii) can be indexed to the djurleite $Cu_{1.94}S$ (i, Fig. S7a), high chalcocite Cu_2S (ii, Fig. S7b) and $MoSe_2$ (iii, Fig. S7c). Noted that the djurleite $Cu_{1.94}S$ (i) and high chalcocite Cu_2S (ii) almost have the same lattice fringes, and the lattice mismatch between the (080) planes of djurleite phase (1.97 nm) and the (110) planes of high chalcocite phase (2.02 nm) is only about 2.5% (Fig. S8). Fig. 1e and f show the Bragg-filtered images from the (080) and (110) reflection of djurleite $Cu_{1.94}S$ (i) and high chalcocite Cu_2S (ii), respectively. The yellow area and green area indicate the presence of djurleite and high chalcocite phase, respectively. Fig. 1d is the HRTEM image taken from the square (iii) in Fig. 1c, the measured lattice fringe (0.66 nm) can be indexed to the (002) planes of $MoSe_2$. In the Bragg-filtered image taken from the (002) reflection of $MoSe_2$ (Fig. 1g), the red areas represent the location of $MoSe_2$ in the $Cu_{2-x}S$-$MoSe_2$ heterostructures. Moreover, the same result can be obtained at the tip of the $Cu_{2-x}S$-$MoSe_2$ heterostructure (Fig. S9). The aforementioned results prove that the $Cu_{2-x}S$ NWs were covered by $MoSe_2$ NSs in the synthesized $Cu_{2-x}S$-$MoSe_2$ heterostructures.

To reveal the detailed interface structure between the high chalcocite Cu_2S (ii) and the grown $MoSe_2$ NSs (iii) in $Cu_{2-x}S$-$MoSe_2$ heterostructures, a series of STEM characterization was

performed (Fig. 2). In the HAADF-STEM images taken from the body (Fig. 2a) and the tip (Fig. 2b) of $Cu_{2-x}S$-$MoSe_2$ heterostructures, it can be seen that $MoSe_2$ NSs closely contact with the high chalcocite Cu_2S with smooth transition cross their interface, indicating the epitaxial growth of $MoSe_2$ NSs on Cu_2S. Importantly, the measured lattice fringe of chalcocite Cu_2S (0.33 nm indexed to the (002) planes) is well matched with that of $MoSe_2$ NSs (0.66 nm indexed to (002) planes). The measured lattice fringes of 0.19 nm and 0.16 nm can be assigned to the $(\bar{1}\,20)$ planes of Cu_2S and $MoSe_2$, respectively. It can be deduced that the epitaxial relationship between the Cu_2S and $MoSe_2$ NSs is $(002)_{Cu2S} \parallel (002)_{MoSe2}$ and $(\bar{1}\,20)_{Cu2S} \parallel (\bar{1}\,20)_{MoSe2}$. Fig. 2c and 2d show the HAADF-STEM and annular bright field STEM (ABF-STEM) images taken at the same area of $Cu_{2-x}S$-$MoSe_2$ heterostructures, respectively. In Fig. 2c, the Mo atoms, indicate by white arrows, can be clearly observed because of their larger atomic number than Se. Noted that the high chalcocite Cu_2S consists of alternating Cu-S and pure Cu layers along the *c* axis.[27] In Fig. 2d, Mo atoms, as indicated by the black arrows, are located between two pure Cu layers of high chalcocite Cu_2S, as indicated by the white dashed lines. It confirms that the Se layers in $MoSe_2$ NSs are closed contacted with the pure Cu layers in the high chalcocite Cu_2S. Since the lattice fringes of (002) planes of $MoSe_2$ (0.66 nm) is well consistent with those of (001) planes of Cu_2S (0.66 nm), i.e. twice that of (002) planes of Cu_2S (0.33 nm) as shown in Fig. 2a, b, it ensures the epitaxial growth of $MoSe_2$ NSs on Cu_2S (Fig. 2e).

In our experiment, the solution of chalcogen precursors was injected by a syringe pump into the mixed solution of $Cu_{2-x}S$ NW seeds, molybdenum precursor and oleylamine. Therefore, the loading amount and lateral size of the formed $MoSe_2$ NSs can be tuned by controlling the injection amount of precursors. Fig. 3a-c illustrate the typical TEM images of $Cu_{2-x}S$-$MoSe_2$ heterostructures obtained at different injection volume of Se precursor solution. With the

increase the volume of Se precursor solution, the lateral size of the grown $MoSe_2$ NSs gradually increase, i.e., 1−2 nm (Fig. 3a), ~5 nm (Fig. 3b) and ~10 nm (Fig. 3c) using 0.5, 1 and 1.75 mL of Se precursor solutions, respectively. The loading amount of $MoSe_2$ NSs on $Cu_{2-x}S$ NWs continuously increases with the injection volume of Se precursor solution. As shown in Fig. 3d and Table S1, the loading amount of $MoSe_2$ NSs can reach 13.6% after 1.75 mL of Se precursor solution were injected.

Impressively, our method can also be used to synthesize $Cu_{2-x}S$-MoS_2 heterostructures by simply changing the Se precursor to S precursor (see Experimental Section for details). Fig. 4a shows a typical TEM image of the obtained $Cu_{2-x}S$-MoS_2 heterostructures, in which MoS_2 NSs are grown vertically along the longitudinal direction of $Cu_{2-x}S$ NWs (see XPS and XRD patterns in Fig. S10 and Fig. S11, respectively). The continuous lattice fringes across the interface between MoS_2 and Cu_2S can be observed in the HAADF-STEM images taken at the tip (Fig. 4b) and body (Fig. 4c) of $Cu_{2-x}S$-MoS_2 heterostructures, indicating the epitaxial growth of MoS_2 on Cu_2S. In Fig. 4c, the measured lattice fringes are 0.64 nm and 0.33 nm, assignable to the (002) planes of MoS_2 and Cu_2S, respectively. More importantly, the Mo layer in MoS_2 (indicated by white dashed arrows) are also located between two pure Cu layers in Cu_2S (indicate by white dashed lines), confirming its same structure as the $Cu_{2-x}S$-$MoSe_2$ heterostructures. The HAADF-STEM image of a typical $Cu_{2-x}S$-MoS_2 heterostructure and the corresponding STEM-EDS elemental maps indicate the existence of Cu, S and Mo elements (Fig. S12), and the uniform growth of MoS_2 NSs on $Cu_{2-x}S$ NWs.

The density and lateral size of the MoS_2 on $Cu_{2-x}S$ NWs also can be systematically controlled by tuning the addition amount of the sulfur precursor solution (Fig. 4 d-g). Fig. 4d-f illustrate the typical TEM images of $Cu_{2-x}S$-MoS_2 heterostructures obtained at different injection volume of S

precursor solution. Noted that quite thick layers of MoS_2 nanosheets covered the entire surface of $Cu_{2-x}S$ NWs can be obtained after 2 mL of sulfur precursor solution was injected (Fig. 4f). Similarly, the loading amount of MoS_2 nanosheets on $Cu_{2-x}S$ NWs also continuously increase with the injection amount of S precursor solution. As shows in Fig. 4g, the loading amount of MoS_2 can be reached at 9.3% after 2 mL of sulfur precursor solution were added.

All the aforementioned results demonstrate the successful construction of epitaxial heterostructures, in which 2D MoS_2 or $MoSe_2$ NSs vertically grown along the longitudinal direction of 1D $Cu_{2-x}S$ NWs. It is different from the previously reported 2D/1D heterostructures in which the orientation of 2D components is random.[28] In our synthesized heterostructures, the well-matched lattice parameters between MoX_2 (or X=S or Se) and Cu_2S ensure the epitaxial growth of high-density 2D MoX_2 NSs on 1D Cu_2S NWs.

Recent studies proved that MoS_2 is a promising co-catalyst alternative to platinum for the photocatalytic hydrogen evolution reaction (HER), owing to its relatively low cost, earth abundance and high catalytic activity.[29-32] In this work, by using the cation exchange method, the $Cu_{2-x}S$-MoS_2 heterostructures with different loading amount of MoS_2 NSs were transformed to CdS-MoS_2 heterostructures. The vertical alignment architecture of MoS_2 on $Cu_{2-x}S$ were well preserved in the obtained CdS-MoS_2 heterostructures, as show in Fig. 5a-c. The successful transformation of $Cu_{2-x}S$-MoS_2 to CdS-MoS_2 heterostructures was further confirmed by XPS, EDS mapping and XRD (Fig. S13-15). Note that the aforementioned CdS-MoS_2 heterostructures cannot be directly synthesized by using CdS NWs as seeds. As a proof-of-concept application, the CdS-MoS_2 heterostructure was used as photocatalyst for HER under visible light irradiation ($\lambda > 420$ nm). Fig. 5d compares the rate of H_2 evolution by using the original CdS NWs and CdS-MoS_2 heterostructures with different loading amounts of MoS_2 NSs as catalysts. Obviously,

pure CdS NWs exhibit negligible catalytic activity (H_2 evolution rate of 79.3 $\mu mol \cdot h^{-1} \cdot g^{-1}$) because of the fast recombination of electron-hole pairs in CdS.[32] In contrast, the CdS-MoS_2 heterostructures show enhanced photocatalytic H_2 production activity due to the recombination delay of electron-hole pairs by MoS_2 NSs. Especially, the CdS-MoS_2 heterostructures with 7.7 wt% of MoS_2 NSs give the highest H_2 production rate of 4,647 $\mu mol \cdot h^{-1} \cdot g^{-1}$, which is about 58 times that catalyzed with pure CdS NWs, and total 114.1 μmol of H_2 were produced after 5 h of reaction (Fig. 5e). Further increasing the loaded MoS_2 cocatalyst, e.g. 9.4 wt%, results in the decrease of the H_2 evolution rate. This might attribute to the high-density MoS_2 layers which could block the light absorption of CdS NWs. Moreover, the photocatalytic stability of CdS-MoS_2 heterostructures with 7.7 wt% of MoS_2 NSs was tested and repeated four times (total 20 h), as shown in Fig. 5f. After four cycles, it does not show significant loss of activity, indicating its good stability for photocatalytic H_2 evolution.

4. CONCLUSION

We have successfully synthesized a unique type of 1D/2D epitaxial heterostructures in which the TMD NSs vertically grown along the longitudinal direction of 1D $Cu_{2-x}S$ NWs in an epitaxial manner. The well matched crystal structures between the TMD and Cu_2S are critical for the successful construction of epitaxial heterostructures. The epitaxial growth of TMD NSs on NWs can facilitate the charge transfer between 2D TMD NSs and 1D NWs, and thus enhance their catalytic performance. Taking the as-obtained CdS-MoS_2 heterostructures as example, they indeed exhibit enhanced photocatalytic activity toward HER under visible light irradiation compared to the pure CdS NWs. We believe that our strategy for the rational design and

synthesis of epitaxial heterostructure offers a new approach for the construction of other TMD-based epitaxial heterostructures, which might have various promising applications.

ASSOCIATED CONTENT

Supporting Information.

The Supporting Information is available free of charge via the Internet at http://pubs.acs.org

This file includes Figure S1-S15, and Table S1.

AUTHOR INFORMATION

Corresponding Author

*hzhang@ntu.edu.sg

*l.gu@iphy.ac.cn

*yu.han@kaust.edu.sa

Author Contributions

‡ These authors contributed equally to this work.

Notes

The authors declare no competing financial interest.

ACKNOWLEDGMENT

This work was supported by MOE under AcRF Tier 2 (ARC 19/15, No. MOE2014-T2-2-093; MOE2015-T2-2-057; MOE2016-T2-2-103) and AcRF Tier 1 (2016-T1-001-147; 2016-T1-002-051), and NTU under Start-Up Grant (M4081296.070.500000) in Singapore. L. G. thanks the financial support from the National Program on Key Basic Research Project (2014CB921002) and the Strategic Priority Research Program of Chinese Academy of Sciences (Grant No. XDB07030200), the Key Research Program of Frontier Sciences, CAS (Grant No. QYZDB-SSW-JSC035) and National Natural Science Foundation of China (51522212, 51421002, 51672307). We would like to acknowledge the Facility for Analysis, Characterization, Testing and Simulation, Nanyang Technological University, Singapore, for use of their electron microscopy facilities.

REFERENCES

1. Cozzoli, P. D.; Pellegrino, T.; Manna, L. *Chem. Soc. Rev*. **2006**, *35*, 1195-1208.
2. Costi, R.; Saunders, A. E.; Banin, U. *Angew. Chem. Int. Ed.* **2010***, 49*, 4878-4897.
3. Zhang, Z.-c.; Xu, B.; Wang, X. *Chem. Soc. Rev.***2014**, *43*, 7870-7886.
4. Choi, C. L.; Alivisatos, A. P. *Annu. Rev. Phys. Chem.* **2010**, *61*, 369-389.
5. Manna, L.; Milliron, D. J.; Meisel, A.; Scher, E. C.; Alivisatos, A. P. *Nat. Mater.* **2003**, *2*, 382-385.
6. Tan, C.; Zhang, H. *J. Am. Chem. Soc.* **2015**, *137*, 12162-12174.
7. Ng, H. T.; Li, J.; Smith, M. K.; Nguyen, P.; Cassell, A.; Han, J.; Meyyappan, M. *Science* **2003**, *300*, 1249-1249.
8. Kim, K. S.; Zhao, Y.; Jang, H.; Lee, S. Y.; Kim, J. M.; Kim, K. S.; Ahn, J.-H.; Kim, P.; Choi, J.-Y.; Hong, B. H. *Nature* **2009**, *457*, 706-710.

9. Bakkers, E. P.; Van Dam, J. A.; De Franceschi, S.; Kouwenhoven, L. P.; Kaiser, M.; Verheijen, M.; Wondergem, H.; van der Sluis, P. *Nat. Mater.* **2004**, *3*, 769-773.

10. Chen, O.; Zhao, J.; Chauhan, V. P.; Cui, J.; Wong, C.; Harris, D. K.; Wei, H.; Han, H.-S.; Fukumura, D.; Jain, R. K. *Nat. Mater.* **2013**, *12*, 445-451.

11. Ma, Y.; Li, W.; Cho, E. C.; Li, Z.; Yu, T.; Zeng, J.; Xie, Z.; Xia, Y. *ACS nano* **2010**, *4*, 6725-6734.

12. Milliron, D. J.; Hughes, S. M.; Cui, Y.; Manna, L.; Li, J.; Wang, L.-W.; Alivisatos, A. P. *Nature* **2004**, *430*, 190-195.

13. Zhang, G.; Yu, Q.; Wang, W.; Li, X. *Adv. Mater.* **2010**, *22*, 1959-1962.

14. Snyder, G. J.; Toberer, E. S. *Nat. Mater.* **2008**, *7*, 105-114.

15. Lim, B.; Jiang, M.; Camargo, P. H.; Cho, E. C.; Tao, J.; Lu, X.; Zhu, Y.; Xia, Y. *Science* **2009**, *324*, 1302-1305.

16. Lee, H.; Habas, S. E.; Somorjai, G. A.; Yang, P. *J. Am. Chem. Soc.* **2008**, *130*, 5406-5407.

17. Geim, A. K.; Grigorieva, I. V. *Nature* **2013**, *499*, 419-425.

18. Huang, X.; Zeng, Z.; Bao, S.; Wang, M.; Qi, X.; Fan, Z.; Zhang, H. *Nat. Commun.* **2013**, *4*, 1444.

19. Schornbaum, J.; Winter, B.; Schießl, S. P.; Gannott, F.; Katsukis, G.; Guldi, D. M.; Spiecker, E.; Zaumseil, J. *Adv. Funct. Mater.* **2014**, *24*, 5798-5806.

20. Tan, C.; Zeng, Z.; Huang, X.; Rui, X.; Wu, X. J.; Li, B.; Luo, Z.; Chen, J.; Chen, B.; Yan, Q. *Angew. Chem. Int. Ed.* **2015**, *54*, 1841-1845.

21. Duan, X.; Wang, C.; Shaw, J. C.; Cheng, R.; Chen, Y.; Li, H.; Wu, X.; Tang, Y.; Zhang, Q.; Pan, A. *Nat. Nanotechnol.* **2014**, *9*, 1024-1030.

22. Gong, Y.; Lin, J.; Wang, X.; Shi, G.; Lei, S.; Lin, Z.; Zou, X.; Ye, G.; Vajtai, R.; Yakobson, B. I. *Nat. Mater.* **2014**, *13*, 1135-1142.

23. Heo, H.; Sung, J. H.; Jin, G.; Ahn, J. H.; Kim, K.; Lee, M. J.; Cha, S.; Choi, H.; Jo, M. H. *Adv. Mater.* **2015**, *27*, 3803-3810.

24. Li, M.-Y.; Shi, Y.; Cheng, C.-C.; Lu, L.-S.; Lin, Y.-C.; Tang, H.-L.; Tsai, M.-L.; Chu, C.-W.; Wei, K.-H.; He, J.-H. *Science* **2015**, *349*, 524-528.

25. Huang, C.; Wu, S.; Sanchez, A. M.; Peters, J. J.; Beanland, R.; Ross, J. S.; Rivera, P.; Yao, W.; Cobden, D. H.; Xu, X. *Nat. Mater.* **2014**, *13*, 1096-1101.

26. Zhang, D.; Wong, A. B.; Yu, Y.; Brittman, S.; Sun, J.; Fu, A.; Beberwyck, B.; Alivisatos, A. P.; Yang, P. *J. Am. Chem. Soc.* **2014**, *136*, 17430-17433.

27. Lukashev, P.; Lambrecht, W. R.; Kotani, T.; Van Schilfgaarde, M. *Phys. Rev. B* **2007**, *76*, 195202.

28. Liu, J.; Jiang, J.; Cheng, C.; Li, H.; Zhang, J.; Gong, H.; Fan, H. J. *Adv. Mater.* **2011**, *23*, 2076-2081.

29. Zhou, W.; Yin, Z.; Du, Y.; Huang, X.; Zeng, Z.; Fan, Z.; Liu, H.; Wang, J.; Zhang, H. *Small* 2013, **9**, 140-147.

30. Zong, X.; Yan, H.; Wu, G.; Ma, G.; Wen, F.; Wang, L.; Li, C. *J. Am. Chem. Soc.* **2008**, *130*, 7176-7177.

31. Chen, J.; Wu, X. J.; Yin, L.; Li, B.; Hong, X.; Fan, Z.; Chen, B.; Xue, C.; Zhang, H. *Angew. Chem. Int. Ed.* **2015**, *54*, 1210-1214.

32. Chang, K.; Mei, Z.; Wang, T.; Kang, Q.; Ouyang, S.; Ye, J. *ACS Nano* **2014**, *8*, 7078-7087.

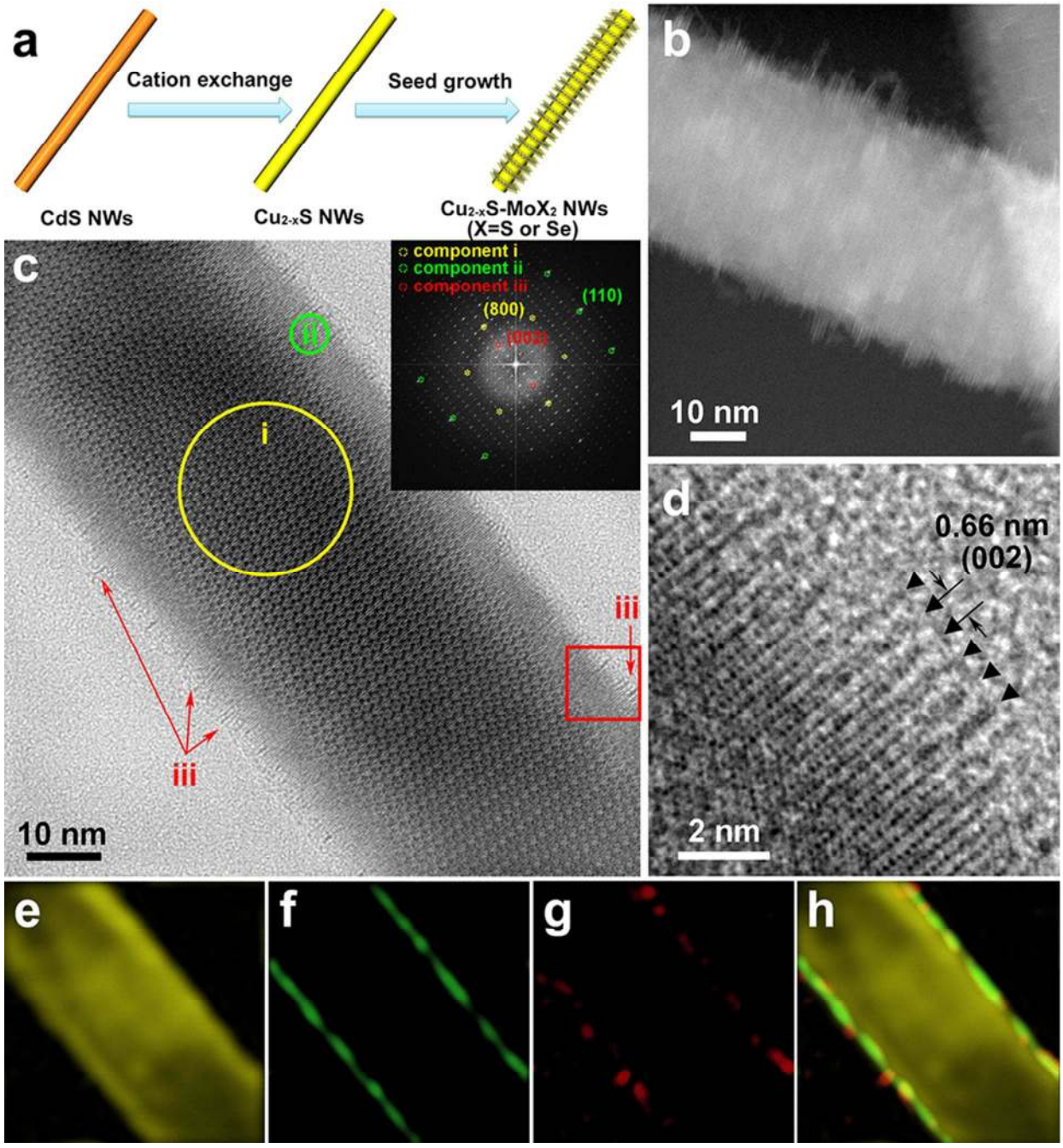

Figure 1. (a) Schematic illustration of the synthesis of $Cu_{2-x}S$-MoX_2 (X=S or Se) heterostructure. (b) HAADF-STEM image of a typical $Cu_{2-x}S$-$MoSe_2$ heterostructure. (c) TEM image of $Cu_{2-x}S$-$MoSe_2$ heterostructure. The circles indicate the $Cu_{1.94}S$, component i and Cu_2S, component ii. The black arrows indicate the $MoSe_2$, component iii. Inset: corresponding FFT pattern of the

$Cu_{2-x}S$-$MoSe_2$. (d) HRTEM image of $Cu_{2-x}S$-$MoSe_2$ taken in the square in (c). (e-g) Bragg-filtered image derived by inverse FFT in component i, ii and iii. The Bragg-filtered images are derived by using the (080) reflection of component i (e), the (110) reflection of component ii (f) and the (002) reflection of component iii (g). The images were then processed with a Sobel filter to enhance their boundaries. (h) Overlap of the Bragg-filtered images of the three components.

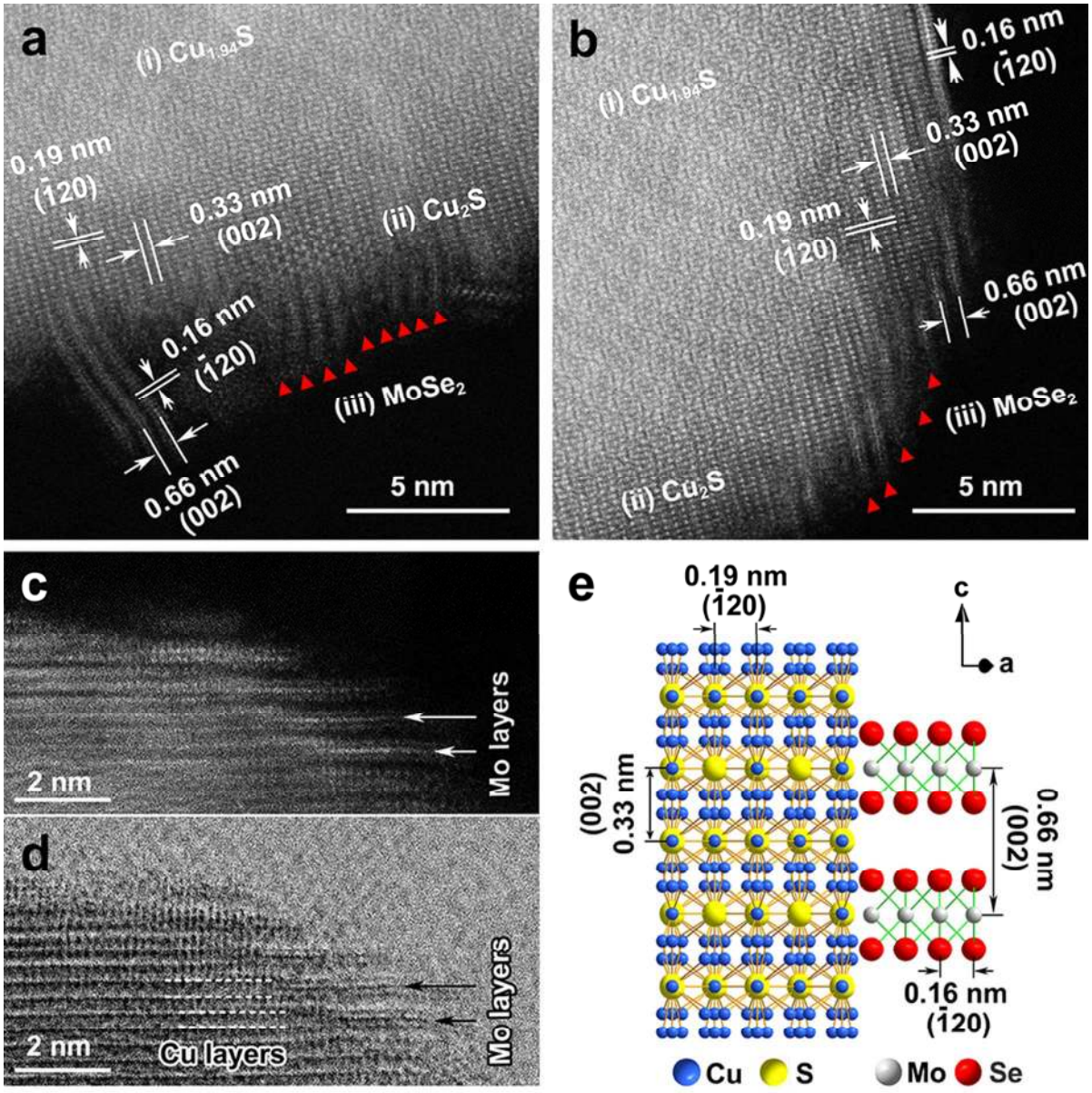

Figure 2. (a, b) HAADF-STEM images of $Cu_{2-x}S$-$MoSe_2$ heterostructures taken at the body (a) and the tip (b) areas. The red triangles indicate the position of $MoSe_2$ NSs. (c) HAADF-STEM and (d) ABF-STEM images of $Cu_{2-x}S$-$MoSe_2$ heterostructures taken at same area. (e) Schematic illustration of the crystal structure of $Cu_{2-x}S$-$MoSe_2$ heterostructures.

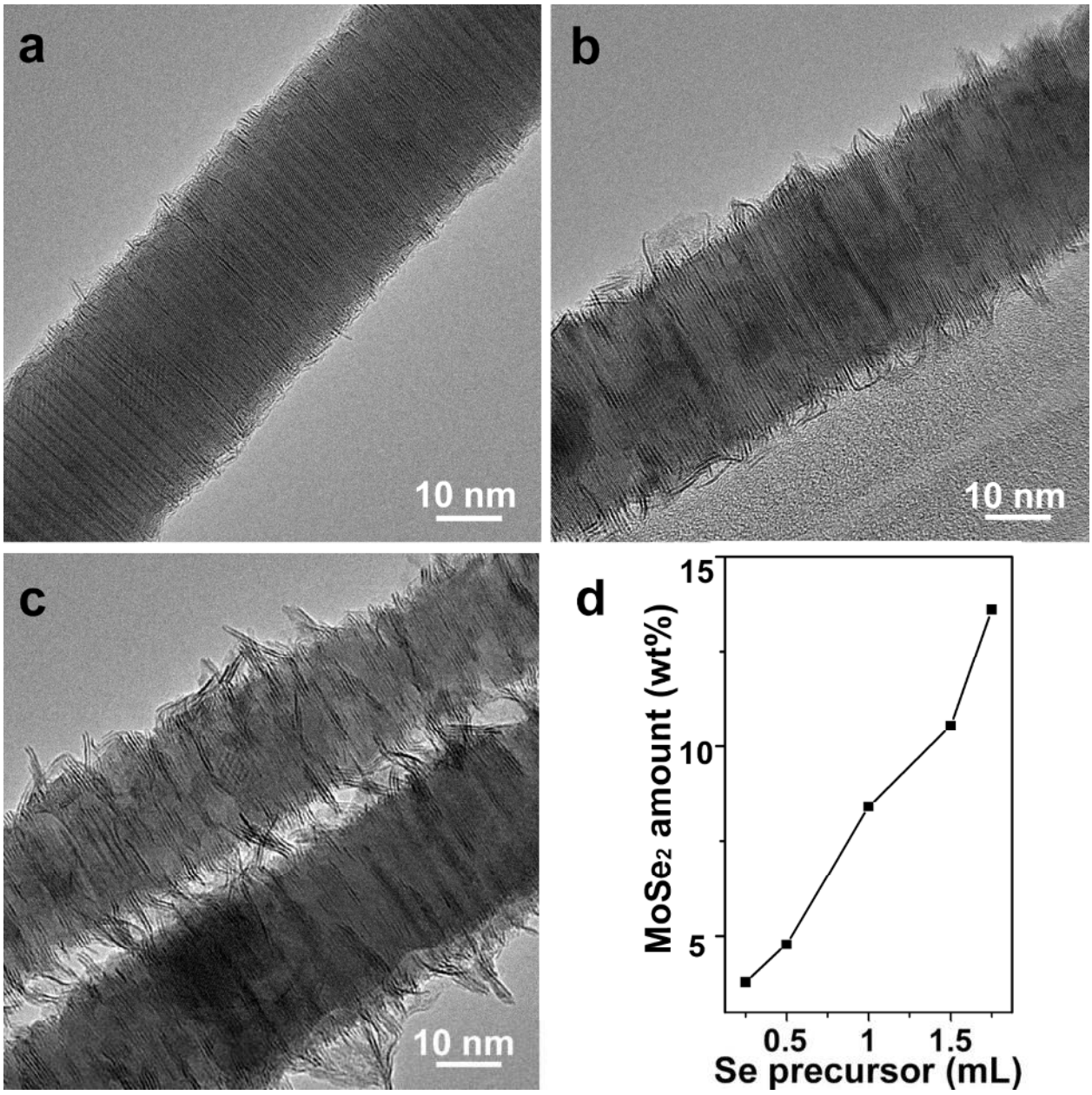

Figure 3. (a-c) TEM images of the $Cu_{2-x}S$-$MoSe_2$ heterostructures obtained at different injection volume of Se precursor solution: (a) 0.5 mL, (b) 1 mL and (c) 1.75 mL. (d) The plot of the weight percentage (wt%) of $MoSe_2$ in $Cu_{2-x}S$-$MoSe_2$ heterostructures, measured by ICP-OES, versus the volume of Se precursor solution.

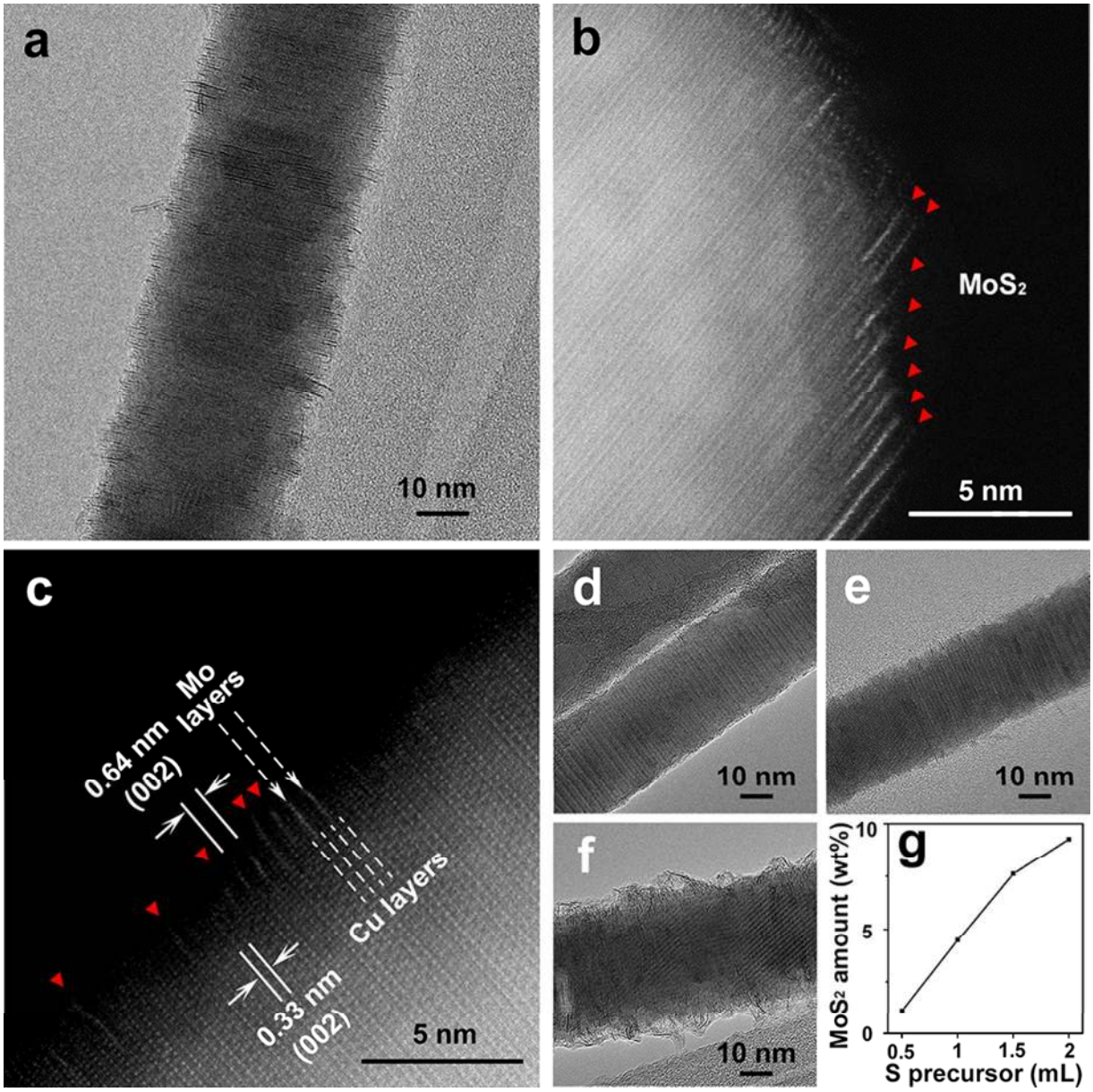

Figure 4. (a) TEM image of a typical $Cu_{2-x}S$-MoS_2 heterostructure, obtained by using 1.5 mL of S precursor solution. (b, c) HAADF-STEM images of $Cu_{2-x}S$-MoS_2 heterostructures taken at the tip (b) and the body (c) parts. The red triangles indicate the position of MoS_2 NSs. (d-f) TEM images of the $Cu_{2-x}S$-MoS_2 heterostructures obtained by using different injection volume of S precursor solution: (d) 0.5, (e) 1.0, and (f) 2 mL. (g) The plot of the weight percentage (wt%) of MoS_2 in $Cu_{2-x}S$-MoS_2 heterostructures, measured by ICP-OES, versus the volume of S precursor solution.

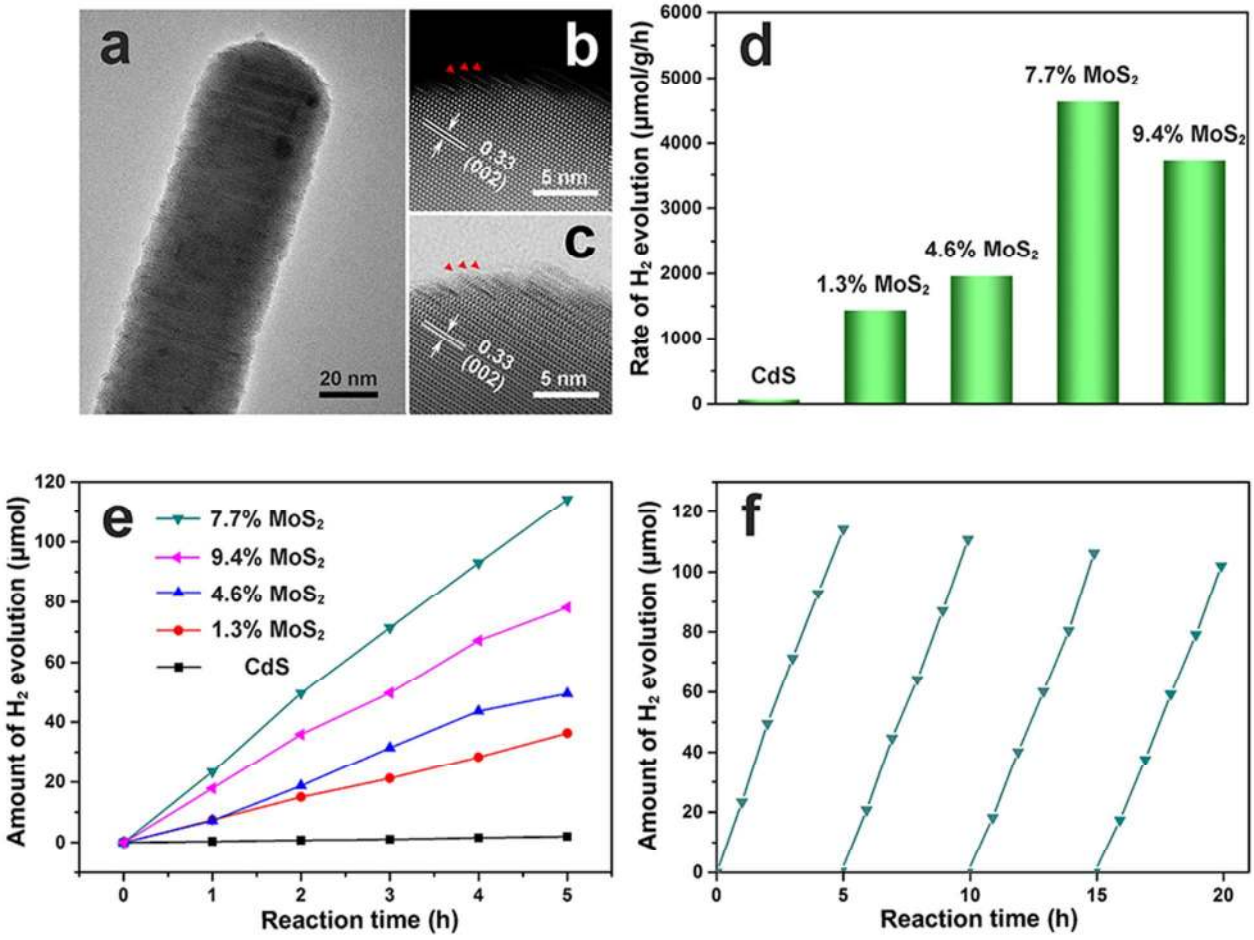

Figure 5. (a) TEM image of CdS-MoS_2 heterostructures. (b) HAADF-STEM and (c) ABF-STEM images of the tip area of CdS-MoS_2 heterostructures. The red triangles indicate the position of MoS_2 NSs. (d) Comparison of H_2 production activities using CdS NW and CdS-MoS_2 heterostructures with different loading amount of MoS_2 NSs as catalysts. (e) Produced H_2 amount after 5 h photocatalytic HERs using CdS NW and CdS-MoS_2 heterostructures with different loading amount of MoS_2 NSs as catalysts. (f) Cycling test of photocatalytic H_2 evolution using CdS-MoS_2 heterostructures with 7.7 wt% MoS_2 NSs as catalyst.

Graphic TOC

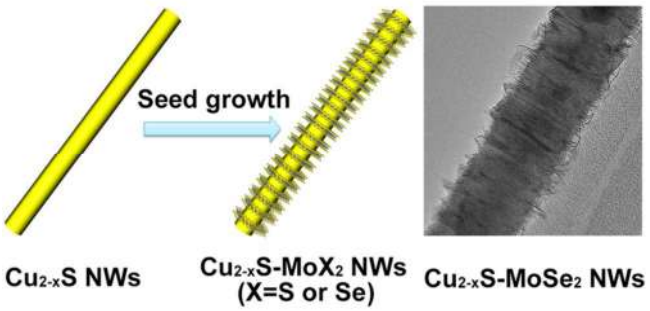

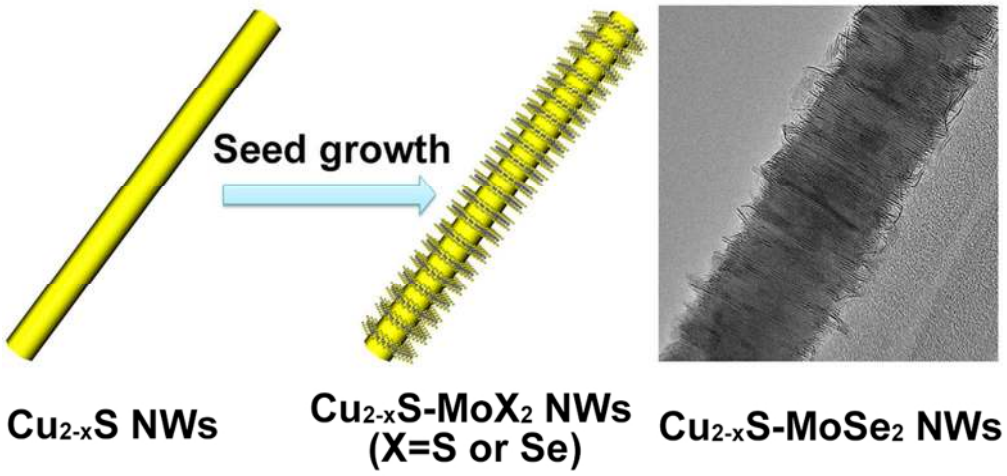

TOC image

85x41mm (300 x 300 DPI)